Effect of La^{3+}/Sr^{2+} ordering on the magnetic properties of $La_{2/3}Sr_{1/3}MnO_3$ by first principles calculations

H´Linh Hmŏk[1,2,3,*], E. Martínez-Aguilar[1,2], J. Ribas-Ariño[4], J. M. Siqueiros Beltrones[3], José Luis Sánchez Llamazares[5], and O. Raymond Herrera[3]

[1]*Computational Laboratory for Advanced Materials and Structures, Advanced Institute of Materials Science, Ton Duc Thang University, Ho Chi Minh City, Vietnam*
[2]*Faculty of Applied Sciences, Ton Duc Thang University, Ho Chi Minh City, Vietnam*
[3]*Centro de Nanociencias y Nanotecnología, Universidad Nacional Autónoma de México, Apdo. Postal 14, Ensenada 22860, Baja California, México*
[4]*Departament de Ciència de Materials i Química Física and IQTCUB, Universitat de Barcelona, Martí i Franquès 1, 08028 Barcelona, Spain*
[5]*Instituto Potosino de Investigación Científica y Tecnológica A. C., Camino a la Presa San José 2055, Col. Lomas 4ª, San Luis Potosí 78216, México*

*Corresponding author e-mails: *hlinh.hmok@tdtu.edu.vn* and *raymond@cnyn.unam.mx*

Abstract

In this work, using DFT+U formalism, we investigate the effect of order-disorder in the A-site occupation by La^{3+} and Sr^{2+} on the stability of the ferromagnetic order in $La_{2/3}Sr_{1/3}MnO_3$ with $R\bar{3}c$ symmetry. To date, a detailed theoretical discussion of such phenomenon, using a combination of different representations of the electronic structure, is still missing in the Literature. We employed structural models consisting of 120 atom supercells constructed according to the precise stoichiometry of the compound. Two configurations, describing randomized and ordered occupation of the La^{3+}/Sr^{2+} ions, were evaluated. We demonstrate that the ferromagnetic arrangement of $La_{2/3}Sr_{1/3}MnO_3$ with randomly distributed La^{3+} and Sr^{2+} ions is more stable. In such configuration we find that the Mn^{3+} and Mn^{4+} ions are not distinguished, favoring the double-exchange mechanism, enhanced by the higher degree of covalence in the Mn-O bonds near the Fermi level between the *spin-up* Mn-e_g orbitals and the O-*p* orbitals.

Keywords: $La_{2/3}Sr_{1/3}MnO_3$ (LSMO), A-site occupation effect, ferromagnetism, first principles calculation, DFT, electronic structure

1. Introduction

The lanthanide manganite doped with strontium, $La_{1-x}Sr_xMnO_3$, has been widely studied in recent decades due to its special magnetic properties and electron transport characteristics. [1-3] In the optimized ferromagnetic composition $La_{2/3}Sr_{1/3}MnO_3$, x = 0.333 (herein LSMO), the spin polarization is greater than 95% and the Curie temperature (Tc) is ~ 370 K, which makes this compound a promising candidate for Spintronics as a source of spin-polarized electron current. [4]

In the perovskite-like structure ABO_3 of $La_{1-x}Sr_xMnO_3$, La^{3+} o Sr^{2+} ions occupy the A site and Mn (Mn^{3+} or Mn^{4+}) ions occupy the B site. The LSMO compound exhibits a ferromagnetic state below Tc, which is generally explained by double exchange interactions between the Mn^{3+} and Mn^{4+} ions. [5-10] In this process, Mn ions transfer electrons through the oxygen ions in the Mn-O-Mn chains, resulting in a simultaneous change of valences between the Mn ions and a ferromagnetic ordering of their magnetic moments.

Presently, many theoretical works have been focused on describing the physical properties of $La_{1-x}Sr_xMnO_3$ with cubic and/or tetragonal perovskite structure. [4, 11-15] A half-metallic bandgap was obtained in the *spin-down* channel for the $PbTiO_3$/LSMO by V. Borisov *et. al.* using the tetragonal structure for the LSMO compound. [11] V. Ferrari *et. al.* used the pseudocubic structure and concluded that the generalized gradient approximation (GGA) offers a qualitatively improved description of the structure and electronic properties of LSMO because it reproduces the half-metal character and gives lattice constants that are in good agreement with experiment. [12] G. Banach *et al.* used the self-interaction corrected local spin density approximation (SIC-LSD) employing the cubic model of $La_{0.7}Sr_{0.3}MnO_3$ and a half-metallic state was obtained with the Mn^{3+} ion configuration, whilst Mn^{4+} behaves like a metallic state. [13] C. Ma *et al.* used GGA in combination with the Hubbard potential (GGA+*U* formalism) with U values between 2 and 3 eV, to obtain the half-metallic behavior of the cubic LSMO in the vicinity of the Fermi level. [4] In addition, they found that the half-metallic character is independent of the chosen substrate and is achieved for all the considered in-plane lattice constants. On the other hand, J. Li *et al.* used the GGA + U formalism for a perovskite cell of LSMO and observed a half-metallic behavior, even with the presence of oxygen vacancy defects. [14] D. Böttcher *et al.* investigated the electronic and the magnetic ground state properties of the LSMO as a function of the tetragonal lattice distortions, using a multiple-scattering Green function method, confirming that the Tc of the ferromagnetic LSMO can be controlled by distorting the crystalline structure. [15]

However, few studies have considered the use of the reported rhombohedral structure belonging to the $R\bar{3}c$ space group, as illustrated with hexagonal axis (see Fig. 1a) and discussed below, to describe the structural, magnetic and electronic behavior of LSMO. In such symmetry the nine coordination of the A-site and the rotation of the MnO_6 octahedron around the [001] direction (rhombohedral [111] direction), are essential differences between the cubic and tetragonal models used for LSMO studies. Meanwhile, Goodenough have demonstrated that for composition x = 0.31 the Mn^{3+} and Mn^{4+} ions are randomly distributed with each Mn^{3+} near to only one Mn^{4+} which must be in correspondence with randomly distributed Sr ions replacing the La ions in the A-site sublattice.[10] Experimentally, D. P. Kozlenko *et al.* showed that the ferromagnetic state of bulk $La_{0.7}Sr_{0.3}MnO_3$ remains $R\bar{3}c$ symmetry stable in the 0-7.5 GPa pressure range.[5] Based on first-principles density-functional calculations and using the GGA, GGA+U and the pseudo-self-interaction correction (PSIC) methods, G. Colizzi *et al.* investigated the structural, electronic and magnetic properties of rhombohedral $La_{0.625}Sr_{0.375}MnO_3$ (x = 3/8 = 0.375) under high hydrostatic pressure.[16] Although the effect of La and Sr ions occupation was not analyzed, G. Colizzi *et al.* used two configurations for the La and Sr ions distribution with 3 Sr ions in a unit cell (with A-site sublattice following a rock salt structure) containing 8 La ions

when undoped: one of them with the Sr placed in a (001)-like plane (its most favored configuration but in opposition to Goodenough theory) and the other with the Sr placed in a (111)-like plane. They found an enhancement of the antiferromagnetic coupling as compression is applied, furthermore, Jahn-Teller (JT) distortions are minimal and symmetry remains roughly rhombohedral even at high pressure. Moreover, experimental and theoretical studies on epitaxial La_2MnNiO_6 thin films, reported by S. R. Spurgeon *et al.*, showed that the ordering of the Mn and Ni ions occupying the B site affect the magnetism of the La_2MnNiO_6 system strongly. [17] They showed that even in the case of layer-by-layer deposition via molecular beam epitaxy, the system growth follows multiple reaction pathways that lead to deviations of the stoichiometry, resulting in Mn-O-Mn and Ni-O-Ni antiferromagnetic monodomain nanoregions, which are detrimental to the expected ferromagnetic ordering where the Mn and Ni ions occupy the B site randomly.

Besides, R. F. Neumann *et al.* used the density functional theory and determined the magnetic properties of the ferromagnetic/antiferromagnetic LSMO/$BiFeO_3$(001) heterojunctions. [18] However, to represent the pseudopotential of La/Sr in LSMO, they used the virtual crystal approximation, replacing the La and Sr atoms by a virtual atom, "LS" atom, whose pseudopotential is a $La_{0.67}Sr_{0.33}$ weighted average of the original pseudopotentials. In summary, a influence of the Sr distribution on the magnetic properties of LSMO has not yet been fully addressed.

Thus, the objective of this work is the theoretical study of the effect of the order-disorder in the A site occupation by La^{3+} and Sr^{2+} on the stability of the ferromagnetic order in $La_{2/3}Sr_{1/3}MnO_3$, using the density functional theory (DFT). To this end, we use structural models corresponding to rhombohedral $R\bar{3}c$ symmetry and containing the exact stoichiometry of the compound, employing two 120-atom unit cell configurations as illustrated in Figs. 1c and 1d, which describe a randomized and an ordered arrangement of the La^{3+}/Sr^{2+} ions occupation, respectively. A detailed analysis of the crystal structure, chemical bonds, and electronic structure were made using the combination of different representations such as the density of electronic states (DOS), band structure, electron density and electron localization function (ELF). A comparative analysis between the reported experimental and theoretical results is also presented.

2. Computational details

The first principles calculations were performed using DFT as implemented in Quantum-Espresso [19]. The projector augmented-wave (PAW) method was used to describe the core pseudopotential. The GGA based on the Perdew-Burke-Ernzerhof (PBE) functional was used for exchange-correlation effects. For a description of the pseudopotentials, 11 valence electrons were selected for the La ($4f^0 5s^2 5p^6 5d^1 6s^2$), 10 for the Sr ($4s^2 4p^6 5s^2$), 15 for the Mn ($3s^2 3p^6 3d^5 4s^2$) and 6 for the O ($2s^2 2p^4$). A plane-wave energy cutoff of 80 Ry was used throughout the calculations. All atomic positions and lattice constants were optimized until the magnitude of the residual energy and force acting on each atom was smaller than 10^{-4} Ry/atom and 10^{-3} Ry/a.u, respectively. The k-point meshes of Monkhorst-Pack $1\times3\times3$ and $3\times9\times9$ were used for geometry structural optimization and electronic structure calculations, respectively. Taking into account the

strong coulombic repulsion between the localized *d*-states of Mn, we use the GGA + *U* approximation to describe the correlation effects in the transition metal oxides.

To evaluate the optimal value of *U* for Mn (U_{Mn}), we take into account as reference the theoretical studies on LSMO that exhibit a half-metallic character with a *spin-down* bandgap of about ~ 2 eV, and maximum values of DOS at energies between -1 and -2 eV below the Fermi energy (E_F) and between 1 and 3 eV above E_F for the Mn-t_{2g} states for *spin-up* and *spin-down*, respectively. [20] Table 1 collects the values of bandgap, magnetic moment of Mn ions, and energy of the maximum of *spin-up* (below E_F) and *spin-down* (above E_F) DOS for Mn-t_{2g} states obtained for different values of U_{Mn}. As can be noted, the *spin-down* maximum of t_{2g} states for $U_{Mn} \geq 4$ eV is outside the reported range from 1 eV to 3 eV, while for $U_{Mn} = 3$ eV, the magnetic moment value of Mn ion is 3.66 μ_B is close to the experimental value of 3.70 μ_B. [20] Therefore, $U_{Mn} = 3$ eV was selected and used for the rest of our calculations.

Table 1. Values of the *spin-down* states bandgap, the magnetic moments of the Mn ions, and the energy of the maximum of Mn-t_{2g} DOS in the *spin-up* and *spin-down* channels for different U_{Mn} values.

U_{Mn} values (eV)	Eg (eV)	M (μ_B/Mn)	t_{2g} (eV) *spin-up*	t_{2g} (eV) *spin-down*
0	1.676	3.38	-1.5866	1.4435
1	2.085	3.47	-1.6731	1.3869
2	2.411	3.57	-1.7198	2.2302
3	2.637	3.66	-1.7190	2.6210
4	3.130	3.76	-1.7315	3.4585
5	3.450	3.86	-1.7091	3.7709

3. Results and discussion

The LSMO hexagonal unit cell (space group 161-$R\bar{3}c$), is illustrated in Figure 1a. Its lattice parameters $a_H = b_H = 5.504$ *Å* and $c_H = 13.351$ *Å*, and the Wyckoff positions of La/Sr *6a* (0.0000, 0.0000, 0.2500), Mn *6b* (0.0000, 0.0000, 0.0000), O *18e* (0.4580, 0.0000, 0.2500), were taken from the data base (ICSD file # 88409).

However, to study how the order or disorder of the A-site occupation by La^{3+} and Sr^{2+} ions affect the magnetic properties of LSMO, and understand the corresponding role of the Mn^{3+} and Mn^{4+} ions distribution on the magnetic interaction mechanism, we used a linear transformation from the hexagonal to a rhombohedral unit cell, herein called construction cell (CC40). This new CC40 unit cell of LSMO, displayed in Fig. 1b, contains 40 atoms (8 La/Sr, 8 Mn and 24 O) with $a = b = c = 7.7587$ *Å*, and $\alpha = \beta = \gamma = 90.37°$, and preserves the $R\bar{3}c$ symmetry. Thus, the $(012)_H$ plane of the hexagonal unit cell corresponds to the $(002)_{CC}$ plane of CC40. In this way, to fulfill the stoichiometry of the $La_{2/3}Sr_{1/3}MnO_3$ compound, for which the La/Sr ratio is 2, we built a larger supercell, which has 120 atoms and consists of three rhombohedral CC40 cells (see Fig. 1c). This new supercell (CC_{ran}) contains 16 La^{3+}, 8 Sr^{2+}, 24 $Mn^{3+/4+}$, and 72 O^{2-} ions. This new supercell contains 16 La^{3+}, 8 Sr^{2+}, 24 $Mn^{3+/4+}$, and 72 O^{2-} ions. Two distinct configurations in terms of the occupation of the A-site by La^{3+} ions or Sr^{2+} ions were considered for this supercell

in order to explore the role of Mn^{3+} and Mn^{4+} ordering: i) a configuration in which the La^{3+} and Sr^{2+} ions were randomly placed in the A-site (CC_{ran}, see Fig. 1c); and, ii) an ordered configuration in which eight Sr^{2+} were placed around a single Mn ion, assuming that this Mn ion behaves like Mn^{4+}(CC_{ord}, see Fig. 1d). Concerning the CC_{ran} supercell, it should be mentioned that, in fact, three different random configurations were initially built. As demonstrated in the Supporting Information, the energy of the three random configurations is very similar. Moreover, the energy difference between the three random configurations is much smaller than the energy difference between any of the random configurations and the ordered configuration (CC_{ord}). For these reasons, we will hereafter consider a single CC_{ran} supercell (the one displayed in Fig. 1c). Moreover, it is known that the magnetic ordering in the crystal structure of the LSMO is established mainly by the alignment of the magnetic moments of the Mn ions. Therefore, in our calculations, we established a collinear arrangement of the magnetic moments of the Mn ions parallel to the *c* direction as illustrated in Figures 1c and 1d.

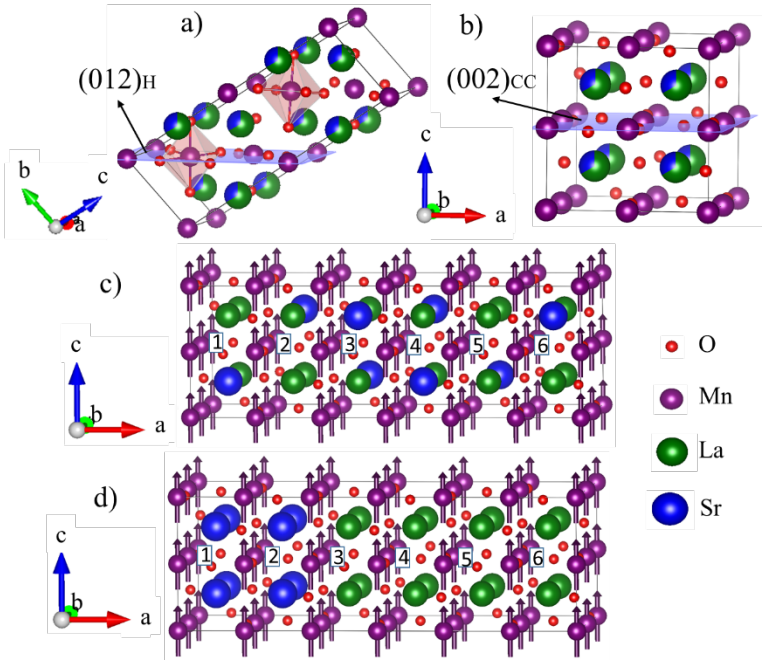

Figure 1. Structure of the LSMO: (a) hexagonal unit cell corresponding to the space group $R\bar{3}c$ (the shadowed MnO_6 octahedrons show their rotation around the [001] direction), (b) rhombohedral construction cell of 40 atoms (CC40), and 120 atom supercell with Sr ions c) randomly (CC_{ran}) and d) ordered (CC_{ord}) distributed.

The results of the structural relaxation for CC_{ran} and CC_{ord} supercells are presented in Table 2. The energy difference between the systems, $\Delta E = E_{CCran} - E_{CCord} = -0.9684$ eV, indicates that the structure with randomly ordered La^{3+} and Sr^{2+} ions is more stable than that with ordered La^{3+} and Sr^{2+} ions. The lattice parameters for CC_{ran} and CC_{ord} cases are similar to each other (see Table 2). However, the lattice angles $\alpha \neq \gamma = \beta$ of the CC_{ran} are slightly larger than those of the CC_{ord}. The average value of the Mn-O bonds is 1.99 Å for CC_{ran} and CC_{ord} cases and slightly

higher than those reported in other works, such as 1.96 Å [16] and 1.954 (2) Å [5]. However, the Mn-Mn distances are not the same for both cases. For comparison, Mn ions are indicated in Fig. 1c and 1d with numbers enclosed in square brackets. In the CC_{ran} case, the distance between the Mn ions remains close to ~3.93 Å. However, for the CC_{ord} case, the distance of Mn1-Mn2 and Mn2-Mn3 is 3.90 Å, while the distance between Mn3-Mn4, Mn4-Mn5, and Mn5-Mn6 is longer, ~3.97 Å. This can be ascribed to the Mn4, Mn5 and Mn6 ions, which are surrounded by La ions, thereby behaving like Mn^{3+} with ionic radius of 0.645 Å. Conversely, the Mn2 ions are surrounded by Sr ions, causing Mn2 to behave like Mn^{4+} with a shorter ionic radius of 0.530 Å with the consequent decrease of the Mn1-Mn2 and Mn2-Mn3 distances. [22] Moreover, taking into account the effective ionic radius of La^{3+} and Sr^{2+} (1.216 Å and 1.310 Å, respectively), we can confirm that the randomness of the A-site occupation for the CC_{ran} develops a homogeneity of the Mn-Mn distance, while the ordered occupation of CC_{ord} generates a non-uniform Mn-Mn distance distribution, which is a difficult situation to obtain experimentally, especially in bulk.

Table 2. Results of structural relaxation for the CC_{ran} and CC_{ord} configurations.

	CC_{ran}	CC_{ord}
Total energy of the system (eV)	-262574.8865	-262573.9181
cell parameters		
a (Å)	23.5766	23.6886
b (Å)	7.8567	7.8641
c (Å)	7.8576	7.8642
γ (a,b) (°)	90.68	90.45
β (a,c) (°)	90.68	90.45
α (b,c) (°)	90.69	90.60
Distance between Mn ions		
Mn1-Mn2 (Å)	3.93	3.90
Mn2-Mn3 (Å)	3.93	3.90
Mn3-Mn4 (Å)	3.92	3.98
Mn4-Mn5 (Å)	3.92	3.97
Mn5-Mn6 (Å)	3.94	3.97
Average distance of Mn-O bond (Å)	1.99	1.99
Distortion angles		
θ (°) [ω (°)]	161.77 [9.12]	162.79 [8.60]

On the other hand, the octahedral distortion can be discussed through the analysis of the θ angle of Mn-O-Mn bonds in the a_{CC}, b_{CC} and c_{CC} directions, and the rotation angle ω of the octahedra related to θ by $\omega = (180° - \theta)/2$. [23] Table 2 summarizes the values obtained from the structural relaxation processes. Similar θ values obtained for CC_{ran} (161.77°) and CC_{ord} (162.79°) are smaller in comparison with the reported experimental values of 166.12° [5], while in correspondence, the octahedral distortion ω is higher than the theoretical values of ω ~7° in agreement with the experimental value [16]. However, the distortion of MnO_6 octahedra in CC_{ran} (ω = 9.12°) is slightly higher than in CC_{ord} (ω = 8.60°). As will be discussed below, this small difference corresponds with the more stable ferromagnetic behavior of the CC_{ran} supercell,

consistent with its lower total system energy, associated with a higher degree of covalence or semicovalence in the Mn-O bonds that promote the double-exchange interactions.

Table 3 shows the magnetic moment values of each labeled Mn ion and the average value for all ions calculated for the CC_{ran} and CC_{ord} cells. Due to the hybridization of the Mn-3*d* and O-2*p* orbitals, the oxygens acquire a finite magnetic moment that tends to be antiparallel to the nearby Mn magnetic moment due to the fact that the Mn-3*d* layer is partially occupied. [16] The average magnetic moment of each ion is equal for both supercells and, as can be noted, the highest magnetic contribution comes from the Mn transition metal ions with an average value of 3.69 μ_B, in good agreement with the reported experimental value of 3.7 μ_B [21].

However, noticeable differences are observed between the magnetic moment values of the individual Mn ions for the CC_{ord} case (Table 3). The magnetic moment value of 3.88 μ_B obtained for Mn5, surrounded by La^{3+} ions, is higher than that of 3.63 μ_B for Mn2 surrounded by Sr^{2+} ions. As expected, this difference can be taken as evidence that the Mn2 surrounded by Sr^{2+} behaves like Mn^{4+} and the Mn5 surrounded by La^{3+} behaves like Mn^{3+}. These results agree with the higher values of magnetic moment reported experimentally for Mn^{3+} ion in $LaMnO_3$ (3.87 μ_B) [24] with respect to those reported for Mn^{4+} ion in $SrMnO_3$ (2.6 μ_B) [25].

Table 3. The magnetic moment values of each labeled Mn ion and average value of the magnetic moments in μ_B units for both cases, CC_{ran} and CC_{ord}.

	CC_{ran}	CC_{ord}
Mn^{3+}/Mn^{4+} average	3.69	3.69
Sr^{2+} average	0.02	0.02
La^{3+} average	0.07	0.07
O^{2-} average	-0.03	-0.03
Mn1	3.73	3.60
Mn2	3.71	3.63
Mn3	3.67	3.60
Mn4	3.68	3.70
Mn5	3.66	3.88
Mn6	3.70	3.70

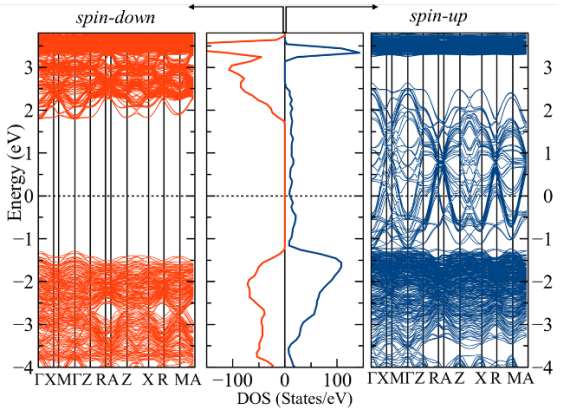

(a)

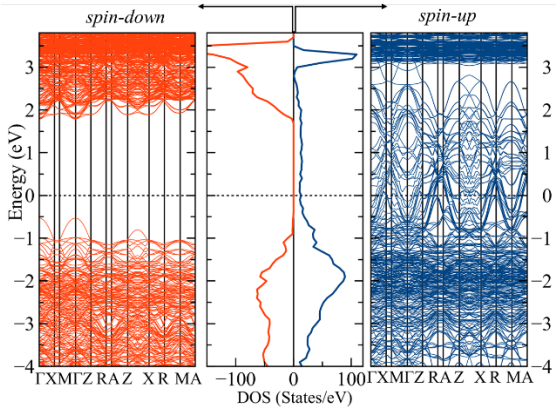

(b)

Figure 2. Band structure and TDOS (in the center part) obtained for (a) CC_{ran} and (b) CC_{ord} supercells.

Figures 2a and 2b present the band structure for the *spin-up* and *spin-down* states and the total density of states (TDOS) of the CC_{ran} and CC_{ord} supercells. The E_F value is set to zero energy. In both cases it is observed that the *spin-up* states exhibit a metallic band structure with states above and below of the Fermi level, while the *spin-down* states show a semiconductor band structure with bandgap values of 2.9 eV for CC_{ran} and 2.6 eV for CC_{ord}. Such features describe the expected half-metal behavior of the LSMO [26].

The TDOS and partial density of states (PDOS) of the Sr^{2+}, La^{3+}, $Mn^{3+/4+}$ and O^{2-} ions for CC_{ran} and CC_{ord} are shown in Figure 3a and 3b, respectively. For both cases, it is observed that the states of the Sr-4*p* and La-5*p* orbitals mainly contribute near -15.3 eV and -14.6 eV, respectively, and do not contribute in the energy region near E_F between -7 eV to 3.8 eV. Meanwhile, as expected for the states of La-4*f*, they contribute in the energy region near below E_F and mainly at higher level in the conduction region above E_F. As can be seen in Fig. 3a, a strong hybridization is observed between the *spin-up* Mn-3*d* and O-2*p* states which mainly occupies all sub-band from -7 eV to E_F indicating the covalence degree of the Mn-O bonds; meanwhile, in such energy region only a contribution of the *spin-down* Mn-3*d* states is observed around -5 eV far from E_F. In addition, near E_F (from -1.26 to 1.64 eV) only the *spin-up* Mn-3*d* and O-2*p* states are present, confirming the half-metal behavior characteristic of the LSMO compound.

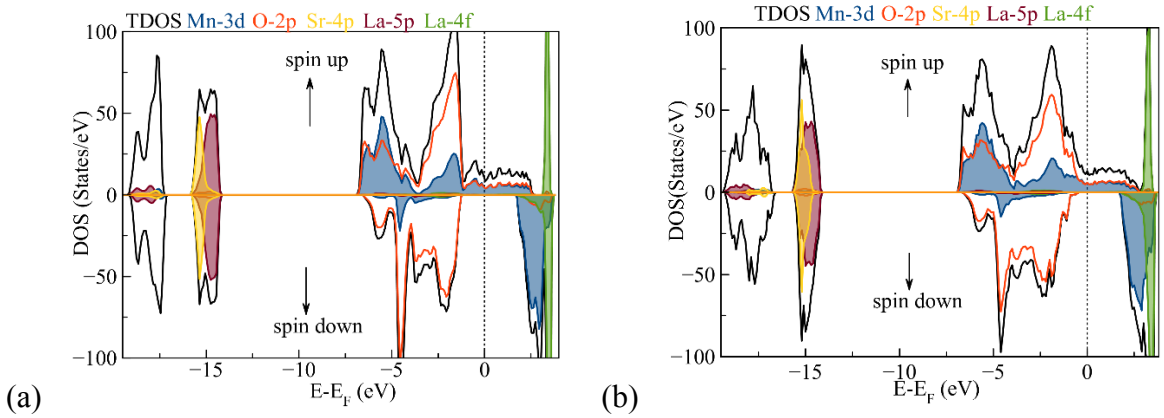

Figure 3. Selected TDOS and PDOS for (a) CC_{ran} and (b) CC_{ord} cells.

To understand better the FM behavior of LSMO, only the deconvoluted PDOS in the region of -2 eV to 3.5 eV for the Mn2 ion (t_{2g} and e_g states) and for their nearest oxygen ions (*p* states) in the MnO_6 octahedron corresponding to the oxygen O_x, O_y and O_z ions, which are along the x, y and z axes, respectively, are shown in Fig. 4a for the CC_{ran} and Fig. 4b for the CC_{ord}. It is observed that the hybridization of the Mn-3d orbitals t_{2g} and e_g states is stabilized only with the P_x, P_y, and P_z orbitals of the oxygen ions that are close to the x, y and z-axis, respectively. It is worth noting that only *spin-up* Mn-e_g states are directionally bonded with such

P_x, P_y, and P_z in the energy region of -1.26 eV to 1.64 eV for CC_{ran}, and of -1.40 eV to 1.70 eV for CC_{ord}. This strong directional hybridization between the oxygen P_x, P_y and P_z orbitals with the *spin-up* Mn-e_g orbital establish a high degree of covalence in the Mn-O bonds near E_F, which enhanced the exchange interactions between the valence states of the Mn ions. Such features are the essential ingredients of the double-exchange mechanism occurrence that causes the FM alignment. [16, 10]

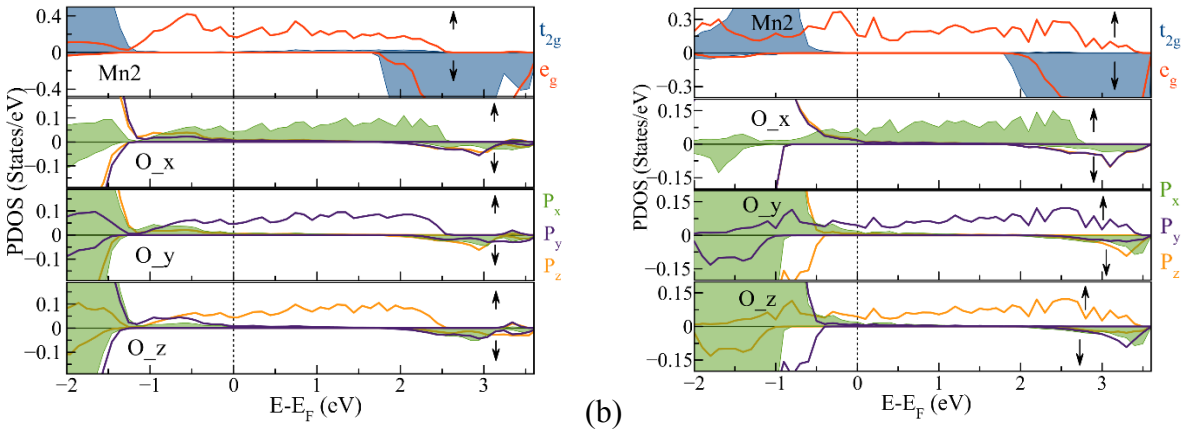

Figure 4. Selected PDOS for the indicated states for (a) CC_{ran} and (b) CC_{ord} cells. O_x, O_y, and O_z are the oxygens surrounding the Mn2 ion in the octahedron along the x, y and z axes, respectively.

Figures 5a and 5c show the PDOS functions of the e_g and t_{2g} orbitals corresponding to the Mn1, Mn2, Mn3, Mn4, Mn5 and Mn6 ions for the CC_{ran} and CC_{ord} models, respectively. Figures 5b and 5d show a close-up of the PDOS functions in Figures 5a and 5c, respectively, in the energy range from -3 eV to 2 eV. For the CC_{ran} case (Figs. 5a and 5b), the PDOS of the e_g and t_{2g} orbitals are very similar for all Mn ions. However, for the CC_{ord} cell (Figs. 5c and Fig. 5d) a shift to energies near E_F of the t_{2g}-PDOS profiles for the Mn2 and Mn3 ions is seen in comparison with the PDOS of other Mn ions. This shift can be associated with the fact that Mn2 in CC_{ord} behaves like Mn^{4+} due to its environment of 8 Sr^{2+} ions, while Mn4, Mn5 and Mn6 behave like Mn^{3+}. Here, we demonstrate that the Mn^{4+} presents a half-metallic state, where the bandgap of the *spin-down* states decreases to 2.6 eV (see Table 4) probably be due to the changes in the Mn-O bond length and the octahedron distortion for Mn2 and Mn3 ions compared with the values of the other Mn ions (see Table 2). This result is different from those reported in Reference 13 where, using an ordered supercell of $La_4Sr_2Mn_6O_{18}$ with cubic symmetry, the authors showed that Mn^{4+} gives rise to a metallic state with a negligible spin polarization at E_F.

Table 4. Bandgap values of the *spin-down* states, and the HOMO and LUMO values in eV for the CC_{ran} and CC_{ord} supercells.

	CC_{ran}			CC_{ord}		
	HOMO	LUMO	Gap, *spin-down*	HOMO	LUMO	Gap, *spin-down*
Mn1	-1.2585	1.6415	2.9	-0.9011	1.6989	2.6
Mn2	-1.2585	1.6415	2.9	-0.9011	1.6989	2.6

Mn3	-1.2585	1.6415	2.9	-0.9011	1.6989	2.6
Mn4	-1.2585	1.6415	2.9	-1.4011	1.6989	3.1
Mn5	-1.2585	1.6415	2.9	-1.4011	1.6989	3.1
Mn6	-1.2585	1.6415	2.9	-1.4011	1.6989	3.1

On the other hand, it is evident that from the PDOS of the CC_{ran} configuration (Fig. 5a and 5b) it is not possible to distinguish between Mn^{3+} and Mn^{4+} ions giving rise to promotion of the double-exchange mechanism between the Mn ions and therefore to the establishment of the FM ordering in the LSMO. However, if the A-site occupation is ordered as the CC_{ord} model, the local stability of the Mn ions with 3+ or 4+ valence, limits the double-exchange occurrence favoring the antiparallel superexchange interactions in detriment of the short range FM coupling.

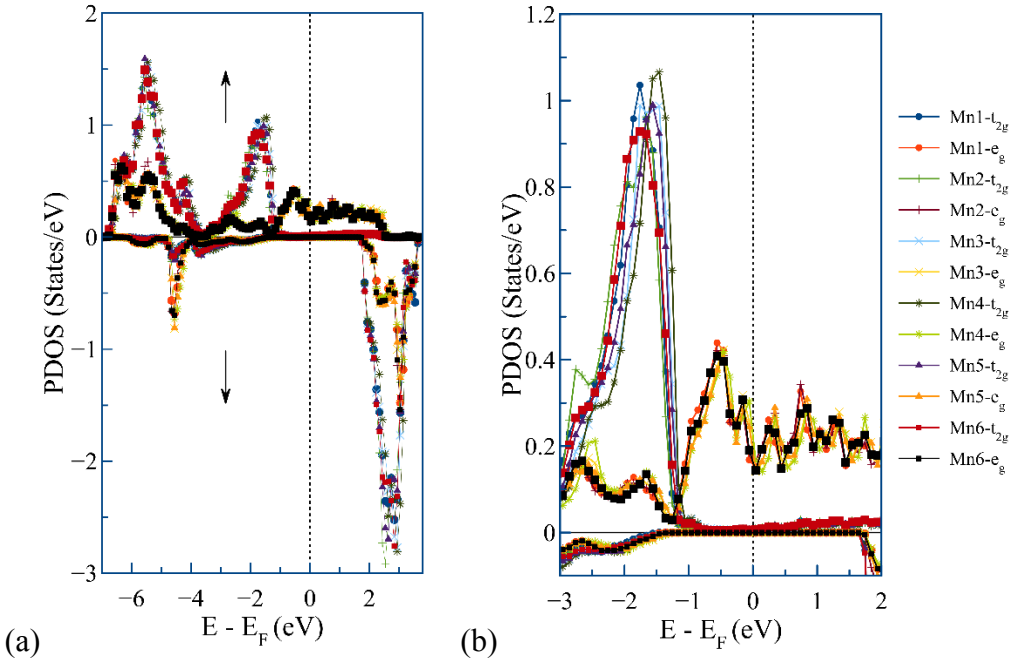

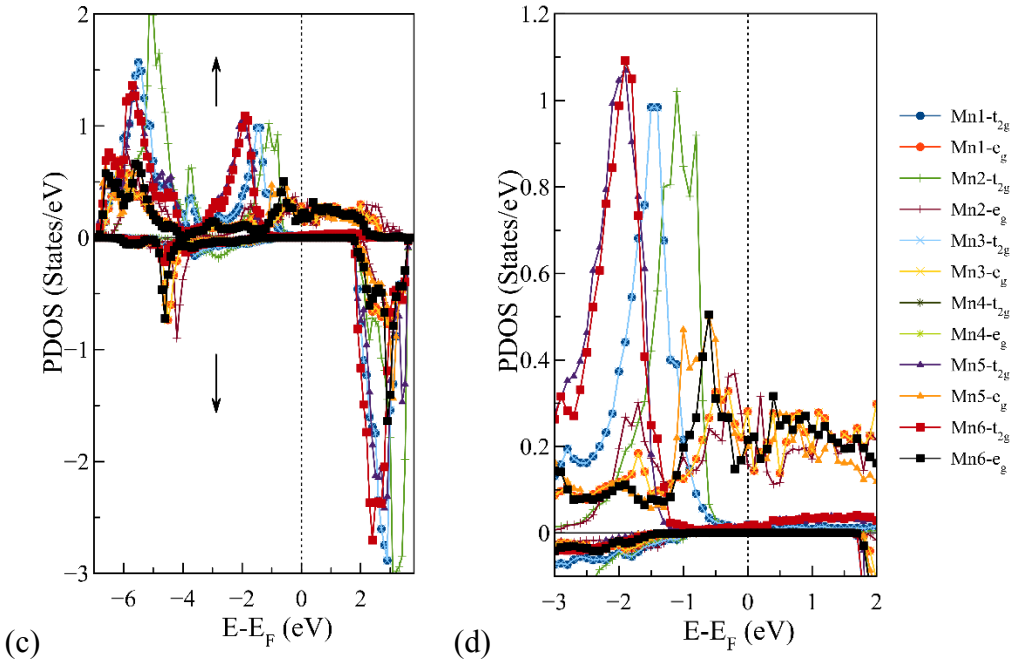

Figure 5. PDOS of the e_g and t_{2g} states of the Mn1, Mn2, Mn3, Mn4, Mn5 and Mn6 ions for (a) CC_{ran} and (b) CC_{ord} supercells. (b) and (d) show a close-up of the PDOS functions (a) and (c), respectively, in the energy range from -3 eV to 2 eV.

In order to distinguish the kind of bonds involved, we use the electronic density representation (ED) and the electron localization function (ELF) analysis. In particular, the ELF provides a measure of the local influence of Pauli's repulsion on the behavior of electrons and allows real-space mapping of the core, bond, and non-crystal regions. [27-28]

Figures 6a and 6b show the ED and ELF functions projected on the $(100)_{CC}$ and $(12\ 0\ 0)_{CC}$ planes for the CC_{ran} case, where it can be seen that a small charge density is shared between the O^{2-} and $Mn^{3+/4+}$ ions. The directional nature of the shared charge distribution between the O^{2-} and $Mn^{3+/4+}$ ions confirms the presence of covalence in the Mn-O bonds as discussed previously in the TDOS and PDOS analysis in Figures 3a and 4a. On the other hand, the charge concentration between the Sr^{2+} and O^{2-} ions is almost negligible, confirming the purely ionic nature of the Sr-O bonds. Meanwhile, it can be observed that the La^{3+} ions partially share their electron density with the O^{2-} ions, which entails an ionic bond with a certain degree of covalence or semicovalence, resulting in an increase of the magnetic moment value of the La^{3+} ions (see Table 3) which in turn, promote an increase in the net magnetic moment of the system.

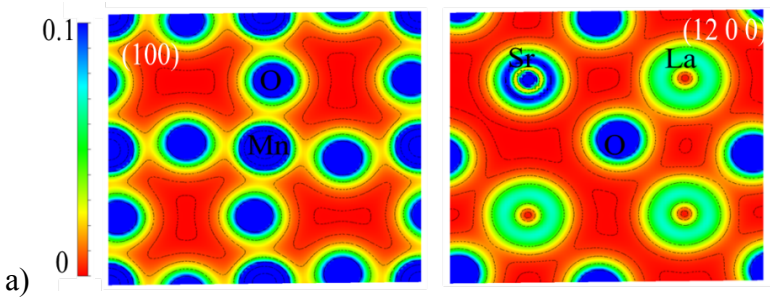

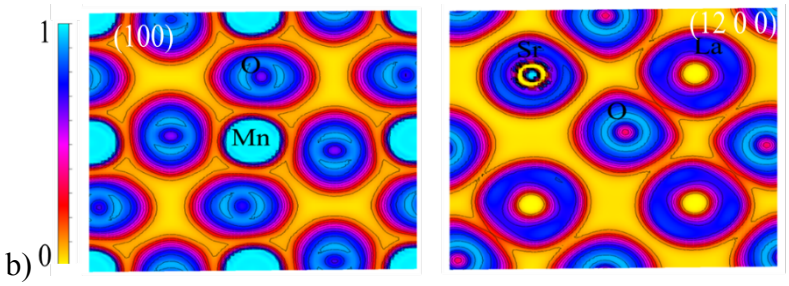

Figure 6. (a) Electronic density and (b) ELF projected on the planes $(100)_{CC}$ and $(12\ 0\ 0)_{CC}$ for the CC_{ran} case.

4. Conclusions

We have successfully investigated the effect of order-disorder in the A-site occupation by La^{3+} and Sr^{2+} on the stability of the ferromagnetic order in bulk LSMO with $R\bar{3}c$ symmetry, using the DFT+U formalism and the Quantum Espresso software package. We have demonstrated that the ferromagnetic arrangement of LSMO with randomly distributed La^{3+} and Sr^{2+} ions is more stable than that with an ordered A-site occupation. With the random configuration, it is not possible to distinguish between the Mn^{3+} and Mn^{4+} ions, thus favoring the double-exchange mechanism, which is enhanced by the high degree of covalence in the Mn-O bonds near the Fermi level between the *spin-up* Mn-e_g orbitals and the O-p orbitals. Conversely, in the ordered configuration, it is possible to distinguish the ions of Mn^{3+} and Mn^{4+}, so the double-exchange mechanism is not favored. It is demonstrated that for the rhombohedral symmetry, Mn^{4+} causes a reduction of the bandgap for the *spin-down* states, nevertheless, the half-metallic nature is maintained. Our work makes clear that for optimal performance of electronic devices making use of LSMO, especially in Spintronics, the random occupancy of the A-site is recommended.

5. Acknowledgments

This work was partially supported by PAPIIT-DGAPA-UNAM Grants IN107918 and IN104320. The authors thank the computer support thorough Projects LANCAD-UNAM-DGTIC-351. The authors thank A. G. Rodriguez Guerrero and P. Casillas for their technical assistance.

References

[1] H. Y. Hwang, S-W. Cheong, N. P. Ong, B. Batlogg, Spin-polarized intergrain tunneling in $La_{2/3}Sr_{1/3}MnO_3$, Phys. Rev. Lett. 77 (1996) 2041-2044. https://doi.org/10.1103/PhysRevLett.77.2041

[2] F. Tsui, M. C. Smoak, T. K. Nath, C. B. Eom, Strain-dependent magnetic phase diagram of epitaxial $La_{0.67}Sr_{0.33}MnO_3$ thin films, Appl. Phys. Lett. 76 (2000) 2421-2423. https://doi.org/10.1063/1.126363

[3] H. M. Albert Gan, K. P. Lim, S. K. Chen, Z. A. Talib, J. K. Wong, Structural, microstructural and electrical properties of $La_{0.67}(Ba,Sr)_{0.33}MnO_3$ system, AIP Conference Proceedings 1328 (2011) 254-256. https://doi.org/10.1063/1.3573746

[4] C. Ma, Z. Yang, S. Picozzi, Ab initio electronic and magnetic structure in $La_{0.66}Sr_{0.33}MnO_3$: strain and correlation effects, J. Phys.: Condens. Matter. 18 (2006) 7717–7728. https://doi.org/10.1088/0953-8984/18/32/019

[5] D. P. Kozlenko, I. N. Goncharenko, B. N. Savenko, V. I. Voronin, High pressure effects on the crystal and magnetic structure of $La_{0.7}Sr_{0.3}MnO_3$, J. Phys.: Condens. Matter 16 (2004) 6755–6762. https://doi.org/10.1088/0953-8984/16/37/011

[6] C. Zener, Interaction between the d-Shells in the Transition Metals. II. Ferromagnetic Compounds of Manganese with Perovskite Structure, Phys. Rev. 82 (1951) 403-405. https://doi.org/10.1103/PhysRev.82.403

[7] P. W. Anderson, H. Hasegawa, Considerations on Double Exchange, Phys. Rev. 100 (1955) 675-681. https://doi.org/10.1103/PhysRev.100.675

[8] P. –G. de Gennes, Effects of Double Exchange in Magnetic Crystals, Phys. Rev. 118 (1960) 141-154. https://doi.org/10.1103/PhysRev.118.141

[9] G. H. Jonker, J. H. Van Santen, Ferromagnetic compounds of manganese with perovskite structure, Physica 16 (1950) 337-349. https://doi.org/10.1016/0031-8914(50)90033-4

[10] John B. Goodenough, Theory of the Role of Covalence in the Perovskite-Type Manganites [La, M(II)]MnO_3, Physical Review 100 (1955) 564-573. https://doi.org/10.1103/PhysRev.100.564

[11] V. Borisov, S. Ostanin, I. Mertig, Multiferroic properties of the $PbTiO_3/La_{2/3}Sr_{1/3}MnO_3$ interface studied from first principles, J. Phys.: Condens. Matter 29 (2017) 175801. https://doi.org/10.1088/1361-648X/aa6318

[12] V. Ferrari, J. M. Pruneda, Emilio Artacho, Density functionals and half-metallicity in $La_{2/3}Sr_{1/3}MnO_3$, phys. stat. sol. (a) 203 (2006) 1437–1441. https://doi.org/10.1002/pssa.200566183

[13] G. Banach, R. Tyer, W. M. Temmerman, Study of half-metallicity in LSMO, J. Magn. Magn. Mater. 272–276 (2004) 1963–1964. https://doi.org/10.1016/j.jmmm.2003.12.1199

[14] J. Li, L. Sun, P. M. Shenai, J. Wang, H. Zheng, Y. Zhao, A first-principles study of oxygen vacancy induced changes in structural, electronic and magnetic properties of $La_{2/3}Sr_{1/3}MnO_3$, J. Alloys Comp. 649 (2015) 973-980. https://doi.org/10.1016/j.jallcom.2015.07.112

[15] D. Bŏttcher, J. Henk, Magnetic properties of strained $La_{2/3}Sr_{1/3}MnO_3$ perovskites from first principles, J. Phys.: Condens. Matter 25 (2013) 136005. https://doi.org/10.1088/0953-8984/25/13/136005

[16] G. Colizzi, A. Filippetti, V. Fiorentini, Magnetism of $La_{0.625}Sr_{0.375}MnO_3$ under high pressure from first principles, Phys. Rev. B 76 (2007) 064428. https://doi.org/10.1103/PhysRevB.76.064428

[17] S.R. Spurgeon, Y. Du, T. Droubay, A. Devaraj, X. Sang, P. Longo, P. Yan, P. G. Kotula, V. Shutthanandan, M.E. Bowden, J.M. LeBeau, C. Wang, P.V. Sushko, S.A. Chambers., Competing Pathways for Nucleation of the Double Perovskite Structure in the Epitaxial Synthesis of La_2MnNiO_6, Chem. Mater. 28:11 (2016) 3814-3822. https://doi.org/10.1021/acs.chemmater.6b00829

[18] R. F. Neumann and M. Bahiana and N. Binggeli, Magnetic properties of $La_{0.67}Sr_{0.33}MnO_3/BiFeO_3(001)$ heterojunctions: Chemically abrupt vs. atomic intermixed interface, EPL 100 (2012) 67002. https://doi.org/10.1209/0295-5075/100/67002

[19] P. Giannozzi et al., Quantum ESPRESSO: a modular and open-source software project for quantum simulation of materials, J. Phys. Condens. Matter 21 (2009) 395502. (http://www.quantum-espresso.org) https://doi.org/10.1088/0953-8984/21/39/395502

[20] J. Jiang, Qing-Ming Chen, X. Liu, First-principles study on the electronic structure and optical properties of $La_{0.75}Sr_{0.25}MnO_{3-s}$ materials with oxygen vacancies defects, Curr. Appl. Phys. 18 (2018) 200-208. https://doi.org/10.1016/j.cap.2017.12.005

[21] M. Ziese et al, Tailoring Magnetic Interlayer Coupling in $La_{0.7}Sr_{0.3}MnO_3/SrRuO_3$ Superlattices, Physical Review Letters 104 (2010) 167203. https://doi.org/10.1103/PhysRevLett.104.167203

[22] Y. Zhou, Z. Lu, S. Xu, D. Xu, Z. Yang, Theoretical Study of Cubic and Orthorhombic $Nd_{1-x}Sr_xMnO_3$ as a Potential Solid Oxide Fuel Cell Cathode, FUEL CELLS 15 (2015) 839–844. https://doi.org/10.1002/fuce.201500050

[23] M. Medarde, J. Mesot, P. Lacorre, S. Rosenkranz, P. Fischer and K. Gobrecht, High-pressure neutron-diffraction study of the metallization process in $PrNiO_3$, Phys. Rev. B 52 (1995) 9248-9258. https://doi.org/10.1103/PhysRevB.52.9248

[24] T. Saitoh et al, Electronic structure of $La_{1-x}Sr_xMnO_3$ studied by photoemission and x-ray-absorption spectroscopy, Phys. Rev. B, 51 (1995) 13942-13951. https://doi.org/10.1103/PhysRevB.51.13942

[25] T. Takeda, S. Ohara, Magnetic Structure of the Cubic Perovskite Type $SrMnO_3$, J. Phys. Soc. Jpn. 37 (1974) 275-275. https://doi.org/10.1143/JPSJ.37.275

[26] J. –H. Park, E. Vescovo, H. –H. Kim, C. kwon, R. Ramesh and T. Venkatesan, Direct evidence for a half-metallic ferromagnet, Nature 392 (1998) 794–796. https://doi.org/10.1038/33883

[27] P. Ravindran, R. Vidya, A. Kjekshus, H. Fjellvåg, and O. Eriksson, Theoretical investigation of magnetoelectric behavior in $BiFeO_3$, Phys. Rev. B 74 (2006) 224412. https://doi.org/10.1103/PhysRevB.74.224412

[28] A. Savin, R. Nesper, S. Wengert, T. F. Fässler, ELF: The Electron Localization Function, Angew. Chem., Int. Ed. Engl. 36 (1997) 1808. https://doi.org/10.1002/anie.199718081